ACS Photonics

JANUARY 2019
VOLUME 6
NUMBER 1
pubs.acs.org/photonics

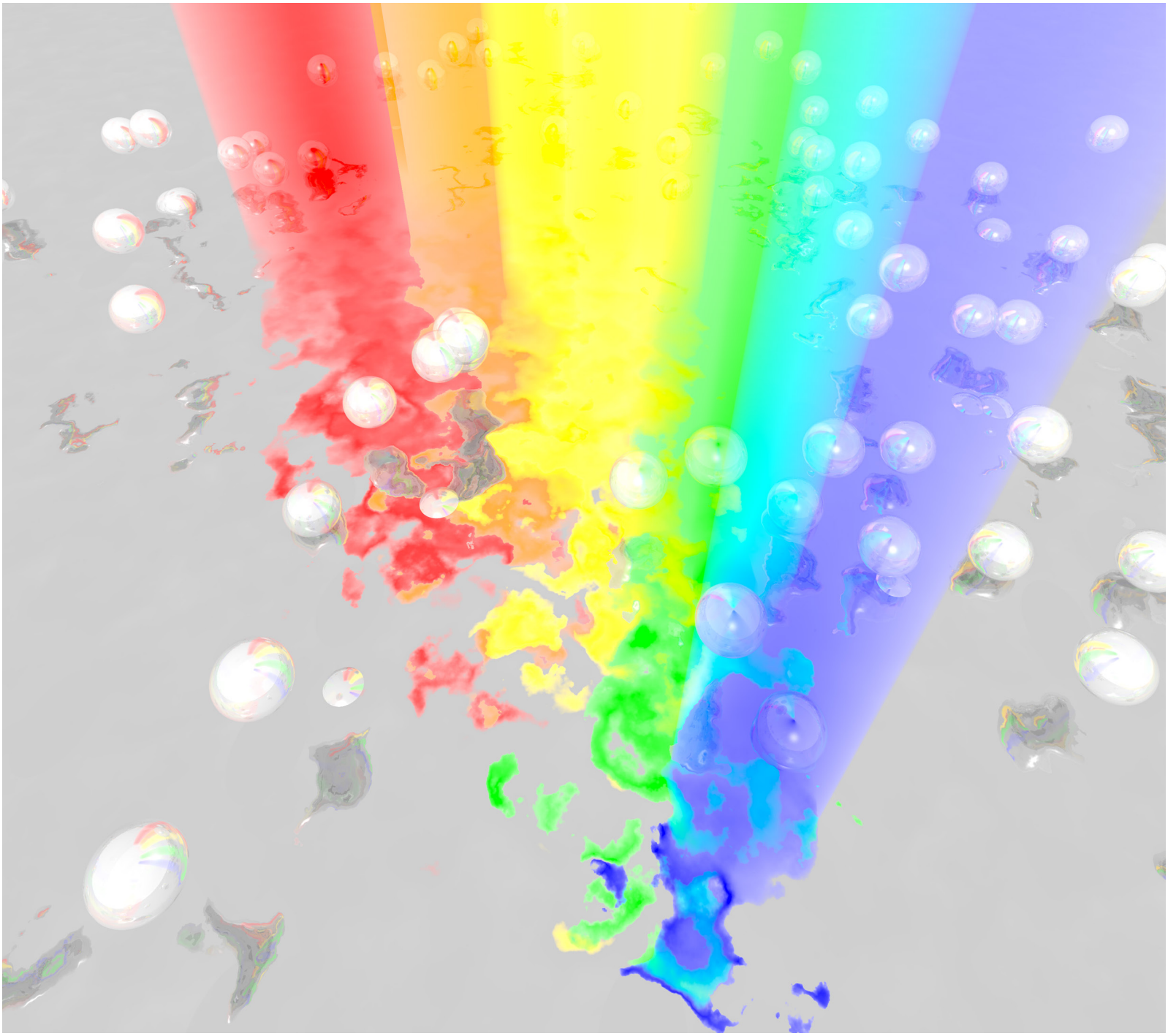

ACS Publications
Most Trusted. Most Cited. Most Read.

www.acs.org

ACS Photonics

Letter

Cite This: ACS Photonics 2019, 6, 272−278

pubs.acs.org/journal/apchd5

Magnesium for Transient Photonics

Thomas G. Farinha,[†,‡] Chen Gong,[†,‡] Zackery A. Benson,[‡,§] and Marina S. Leite*[,†,‡]

[†]Department of Materials Science and Engineering, University of Maryland, College Park, Maryland 20742, United States
[‡]Institute for Research in Electronics and Applied Physics, University of Maryland, College Park, Maryland 20742, United States
[§]Department of Physics, University of Maryland, College Park, Maryland 20742, United States

Supporting Information

ABSTRACT: Optical reconfigurability has enabled the realization of photonic devices that change in functionality, including modulators, sensors, and signal processors. Yet, most approaches to date require the application of power, which severely limits their usage in portable devices. We demonstrate the concept of transient photonics based on Mg, a burgeoning material for (nano)photonics. We realize dynamic Mg/MgO/Mg color pixels covering the entire sRGB gamut color spectrum, where all hues vanish completely in less than 10 min upon exposure to water at room temperature and neutral pH, ideal for encryption. This scalable thin-film architecture has a robust angular response, maintaining vivid colors up to 80 degrees of incidence. Our transient photonics approach using materials that are earth-abundant and CMOS-compatible opens the door for the implementation of reconfigurable devices with controlled responses in the UV−IR that can disappear without leaving any trace after stable operation, relevant for healthcare, defense, and energy applications.

KEYWORDS: *transient photonics, reconfigurability, dynamic optical response, magnesium, color pixels, earth-abundant materials for photonics*

The ability to control the optical behavior of metals has enabled the development of photonic devices ranging from color pixels for displays[1−3] and nanolasers[4,5] to superabsorbers[6−8] and novel designs for photovoltaics,[9,10] Recently, the necessity for devices with tunable functionality has triggered the search for materials and architectures that allow optical reconfigurability, e.g., change in light absorption, reflection, and transmission. Up until now, the pathways for achieving reconfigurability have been based on modifying the materials' electrical and/or optical properties, including the application of bias or carrier injection,[11] selective light polarization,[2] mechanical actuation,[12] and strain.[13] Concerning materials commonly implemented in reconfigurable photonics, most approaches are based on VO_2,[13,14] where a change in temperature of >40 °C is responsible for the transition between a dielectric (low temperature) and a metal (high temperature).[14] Regarding emerging optical materials, changes in chemical composition can also allow for reconfigurability. Specifically, the hydrogenation of Mg nanostructures capped by a Pd layer has been recently shown to be an effective knob for color tunability, resulting from the reversible shift between Mg (metallic) and MgH_2 (dielectric behavior) upon hydrogenation and dehydrogenation.[15,16]

The extensive research performed with Ag, Au, Al, and Cu,[17,18] as well as their combinations,[6,19−23] has proven that engineered permittivity can be achieved in the vis−NIR range of the electromagnetic spectrum. Nevertheless, Ag and Au are neither CMOS-compatible nor earth-abundant. These constraints prompted intense investigation of ceramic materials, such as TiN,[24] and intermetallics,[23] which present low optical losses in the NIR. The search for photonic devices that operate at optical frequencies motivated the development of Al for plasmonics in the past few years.[1,25,26] Al is the third most abundant material on the earth's crust and, therefore, is low-cost, CMOS-compatible, and also low density (2.70 g/cm^3), facilitating portable applications. Further, different from Ag and Au, the plasmon resonances in Al extend into the UV because this metal does not contain interband transitions at short wavelengths.[26] Although Al easily forms a self-passivating Al_2O_3 oxide layer of ∼3 nm,[27] it still has resonance tunability through nanostructuring. As a result, thin-film and nanostructured Al have been shown to be working components in color-selective detectors,[1,28] polarization-dependent color palettes for encoding,[2] scattering centers for solar cells,[29] nanoantennae,[25] photocatalysts,[27] etc. While Al presents a set of suitable characteristics for photonics, it is not biocompatible, and it cannot disintegrate under ambient conditions.[30] For many applications, including communication and sensing, a "holy grail" objective in photonics is to create optical devices that can (i) hide and reveal sensitive information *on demand* for encryption, (ii) vanish as needed after stable operation without leaving any trace, and (iii) be swallowed by humans if required (with confirmed biocompatibility). To date, most efforts in the blossoming field of transient photonics have focused on using silk[31−33] and polymers,[34] which can be unstable upon exposure to UV radiation, hindering the lifetime of the devices. Hence, we propose a platform for transient photonics using Mg (metal) and MgO (dielectric), which are

Received: September 13, 2018
Published: December 4, 2018

DOI: 10.1021/acsphotonics.8b01299
ACS Photonics 2019, 6, 272−278

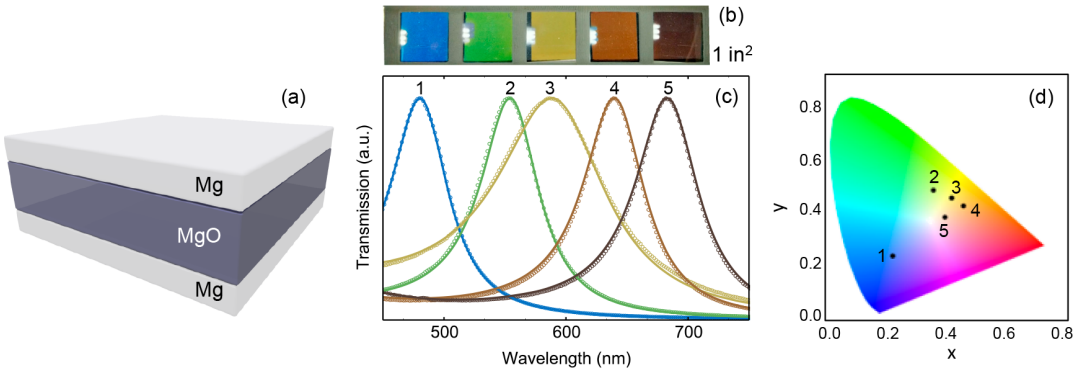

Figure 1. Mg-based color pixels with full RGB gamut. (a) Schematic illustration of scalable Mg/MgO/Mg color pixels for transient photonics. (b) Photographs of 1 by 1 in.^{2} samples with variable MgO thicknesses, which provide colors varying along the visible range of the electromagnetic spectrum. (c) Measured (open circles) and calculated (solid line) transmission spectra of the color pixels. (d) CIE 1931 space chromaticity diagram with the fabricated pixels indicated by #1 to #5.

stable under ambient conditions, earth-abundant, biodegradable, and biocompatible materials.

In this Letter, we demonstrate a novel material system for transient photonics based on Mg (metal) and MgO (dielectric), both earth-abundant and CMOS-compatible. We realize scalable color pixels formed by metal−insulator−metal (MIM) stacks composed by Mg/MgO/Mg, where the colors vanish in less than 10 min when exposed to water, at room temperature and neutral pH. These pixels present vivid chromaticity as a result of constructive interference and can encompass the entire color gamut, varying from blue to red, depending on the thickness of the middle MgO layer. Our experiments and calculations show that the full standard red green blue (sRGB) color space diagram can be obtained, including yellow (often not achievable by MIM). This scalable thin-film deposition and the low-cost materials utilized are ideal for coating applications. The dynamic behavior of our color pixels is validated by etching the MIM structures in water, under ambient conditions. The hues disappear in minutes when the samples are etched in water, confirming the optical transiency of the devices, a very valuable characteristic for encryption. We provide a detailed analysis of the color changes that take place while the MIM devices are exposed to water, where distinct hues are found to contribute to the final hue observed. The pixels are omnidirectional with respect to hue up to 40 degrees and provide bright colors up to 80 degrees. Our results lay the foundation for stable and transient photonics based uniquely on low-cost and nontoxic materials. Thus, we foresee the development of game-changing devices for zero-power reconfigurability, including transient modulators, sensors, beam steers, and optical filters, all based on the controlled dissolution of Mg and MgO in water.

Mg is a material with unique properties: it can vanish in water (at room temperature and neutral pH), has ultralow optical losses,[35,36] is earth-abundant (eighth most abundant element on Earth), conducts electricity, is paramagnetic, is CMOS compatible, has very low density (1.738 g/cm^3, suitable for portable devices), is biodegradable and biocompatible,[30] and can be fabricated into thin films[35] and nanostructures.[37,38] Concerning the optical properties of Mg, its permittivity shows an ε_1 similar to Al[39] (up to ~1300 nm, see Figure S1), without the interband transitions well known for causing losses in both Ag and Au. The imaginary part of the permittivity (ε_2), primarily responsible for light absorption, is lower than that of Al up to 934 nm, where ε_2 quickly increases with wavelength. Thus, Mg is an ultra-low-loss material in the UV−vis range of the spectrum, outperforming Ag, Au, and Al. Different from Al, Ag, Au, and Cu, Mg is water-soluble. Thus, devices can completely disintegrate upon exposure to water. The chemical reactions of both Mg and MgO with water (at room temperature and neutral pH) result in the production of magnesium hydroxide [$Mg(OH)_2$], a mineral commonly found in nature in the form of brucite and a compound used as an active ingredient in milk of magnesia (with confirmed biocompatibility). These reactions are described in eqs 1 and 2):

$$Mg_{(s)} + 2H_2O_{(l)} \rightarrow Mg(OH)_{2(s)} + H_{2(g)} \quad (1)$$

$$MgO_{(s)} + H_2O_{(l)} \rightarrow Mg(OH)_{2(s)} \quad (2)$$

$Mg(OH)_2$ is found naturally in several countries, making it easily untraceable when disposed. Moreover, both Mg and MgO are stable under UV light and can be fabricated into nanostructures, ideal for metamaterials and metasurfaces with dynamic magnetic responses and tunable chirality upon controlled exposure to water. Considering all aforementioned physical and chemical properties and the very low cost of Mg (US $3.7 per 100 g, compared to > US $48.0 for Ag and US $3,800 for Au), we propose Mg and MgO as a novel platform for zero-power reconfigurable photonics, which enable devices to change their optical response or disappear on demand, ideal for hiding highly secure information (encryption).

We implement Mg/MgO/Mg MIM stacks for transient and low-cost color pixels for sRGB, as illustrated in Figure 1. The vivid, full-color gamut is obtained by varying the thickness of the MgO middle layer (from 92 to 153 nm), resulting in constructive interference.[40] The advantage of this fabrication method is that it is easily scalable, not requiring the use of e-beam lithography or templated deposition (no need to nanostructure the surface of the films), making it very suitable for coating applications. Figure 1b,c shows photographs and the transmission spectra of five representative 1 in.^{2} pixels. The thicknesses of each layer are presented in Table S1. The measured and calculated transmission data (open circles and solid lines, respectively) are in excellent agreement. The transmitted spectra show full-width-half-maximum (fwhm) values as narrow as 54 nm in some cases. As presented in Figure 1d, we can achieve the entire portion of the CIE 1931

DOI: 10.1021/acsphotonics.8b01299
ACS Photonics 2019, 6, 272−278

color diagram required for pixel displays by varying the thickness of the MgO middle layer. Here, the fabricated hues are indicated by #1 to #5. For the electric field intensity distribution of all five MIM stacks as a function of depth and wavelength, refer to Figure S2.

All colors from the sRGB gamut can be obtained by simply changing the relative thicknesses of the Mg and MgO layers, potentially delivering all hues in the full chromaticity diagram for use in displays. As a proof-of-concept, we fabricate the pixels indicated by the square symbols in Figure 2, which

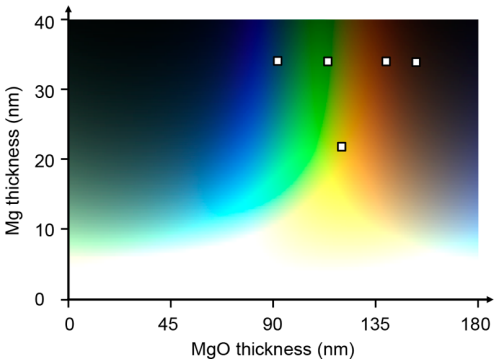

Figure 2. Mg and MgO for full chromaticity diagram. Calculation of transmitted color as a function of Mg (*y*-axis) and MgO (*x*-axis) layer thicknesses in a Mg/MgO/Mg configuration. All hues are obtained by using the transmission spectra of the MIM stacks and the respective CIE color matching functions. The square symbols indicate the Mg and MgO thicknesses of the fabricated pixels.

shows the calculated transmitted hues that can be realized by MIM stacks composed of Mg (*y*-axis) and MgO (*x*-axis). Note that it is difficult to achieve vivid yellow with our thin-film MIM structures, as the window for accessing this hue is extremely narrow. For Mg top layers > 30 nm, reflection from the metallic layer results in poor light absorption. As this top layer becomes optically thick (i.e., a mirror), no color is generated. Yet, by decreasing the thickness of the Mg top and bottom layers from 34 nm to 22 nm we attain bright yellow pixels (see also Figure 1b,c). Despite the broader fwhm of this sample (100 nm, as presented in Figure 1c), a bright and vivid hue is still attained. A thickness threshold for both materials is required to provide color, where a lower bound occurs for 8–10 nm of Mg. The white region of the map presented in Figure 2 indicates this situation. Very thin (<45 nm) and very thick (>150 nm) MgO layers combined with metallic layers with thicknesses above 20 nm result in a dark gray hue in the visible range of the spectrum, as a consequence of light absorption. Our calculations can be used as a design guide for color pixels.

In Figure 3 we present the unique transient optical response of Mg-based color pixels. The MIM stacks vanish by exposing them to water (at room temperature and neutral pH), demonstrating our concept of reconfigurability. Snapshots of the dissolution of Mg on water are presented in Figure S3. After 2 min the hues are still present, but less vivid than the original samples, due to the reduced Mg layer. Within 4 min, the yellow color essentially disappears, as it refers to a thinner metal layer (etches faster). Simultaneously, all other pixels have their original color barely preserved. At 8 min of etching in water, all original colors vanish completely (see supplementary video for real-time experiment), and all pixels look similar. This fast change in chromaticity (see Figure S4) is particularly valuable for encryption, where sensitive information could be quickly erased if needed, without the need of any power sources in this case. In such situations, water or urine (with an average pH of ~6.2) would be sufficient to erase the information being stored by the Mg/MgO/Mg pixels. Further, if the MIM is deposited on poly(vinyl alcohol) (PVA, a biocompatible substrate that also dissolves in water), the entire device could disappear without leaving *any* trace or even be swallowed by humans if needed. Dynamic optical responses have also been shown using metallic nanostructures, such as Al,[41] Ag,[42,43] and Mg, as well as high-index dielectric metasurfaces.[44] These approaches generally rely on either changing the material, e.g., its chemical composition or its mechanical configuration, or selective light polarization. A primary advantage of our paradigm is that it is "zero-power", i.e., there is no need to change the material itself or the light source. Moreover, our thin-film architecture enables straightforward scalability, different from the vast majority of nanostructuring fabrication routes.

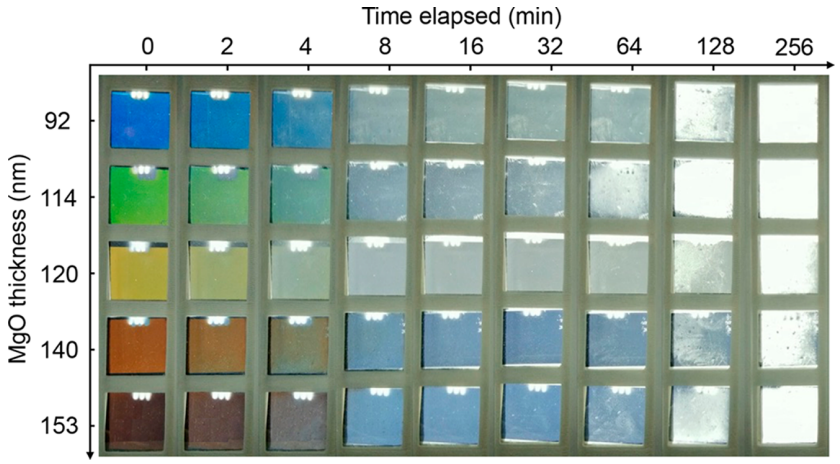

Figure 3. Transient color pixels. Snapshots of Mg/MgO/Mg color pixels with 1 in.^{2} area covering the full chromaticity gamut as it dissolves in water, at room temperature (23 °C) and neutral pH. The photographs are obtained by back illuminating the samples with a white light source and, thus, refer to the transmitted light.

DOI: 10.1021/acsphotonics.8b01299
ACS Photonics 2019, 6, 272–278

The dynamic optical behavior of the Mg-based color pixels is further analyzed by calculating the chromaticity variations as a function of exposure to water, until both Mg and MgO react completely (and all hues totally vanish). In Figure 4 we display each color change, from the initial thickness of each MIM stack (and original color) through their pathway until they completely vanish and all material dissolves in water. The time-dependent, dynamic behavior of the MIM stacks is generated using the transmission response resulting from water exposure (and the changes in thickness). We assume periodic x-direction and perfectly matched layer y-direction boundaries for all calculations, with a broadband light source comprised of 471 equally spaced wavelengths ranging from 360 to 830 nm, to match the wavelength range for the CIE 1931 color space. The initial thicknesses for each metallic and dielectric layer are selected based on the experimental data presented in Table S1. Then, we calculate the etching effect by computing the transmission intensity as a function of wavelength for every MIM stack thickness between its original maximum value and zero, where the overall thickness is reduced by "removing" material from its top in increments of 0.5 nm. In the calculations, we assume that both the original MIM stack and all etching snapshots are flat (with no roughness), which could produce slight color variation in comparison to the experimental MIM stacks (see Figure 3). In particular, the hues formed upon the partial removal of the top Mg layer on both green and yellow pixels cannot be observed in our experiments. This happens because as the Mg top layer is etched, it becomes rougher (5.6 nm) than the original films (<1.6 nm, see Figure S5), and the color changes for the pixels correspond to a very narrow range in thickness: 6 and 5 nm, respectively. We convert the transmission vs wavelength data corresponding to a specific MIM thickness into equivalent CIE 1931 tristimulus XYZ values by matching the CIE 1931 (2° observer) data to every wavelength and multiplying the Y value by the relative transmission intensity for each respective wavelength. Y represents the luminance of each color, where a luminance factor L represents the effect of transmission filtering. These XYZ tristimuli are then converted into xyz chromaticity coordinates using the following equations:[45]

$$x = \frac{X}{X + Y + Z,}\ y = \frac{Y}{X + Y + Z,}\ z = \frac{Z}{X + Y + Z}$$

$$x + y + z = 1$$

The x and y chromaticity coordinates for all wavelengths in a specific MIM stack thickness are then combined using the equations[45] below to determine their equivalent color with the mixture x and y chromaticity coordinates x_m and y_m, respectively.

$$x_m = \frac{\left(\frac{x_1}{y_1}L_1 + \frac{x_2}{y_2}L_2 + +\frac{x_3}{y_3}L_3 \ldots + \frac{x_n}{y_n}L_n\right)}{\left(\frac{L_1}{y_1} + \frac{L_2}{y_2} + \frac{L_3}{y_3} + \ldots + \frac{L_n}{y_n}\right)}$$

$$y_m = \frac{(L_1 + L_2 + L_3 + \ldots + L_n)}{\left(\frac{L_1}{y_1} + \frac{L_2}{y_2} + \frac{L_3}{y_3} + \ldots + \frac{L_n}{y_n}\right)}$$

The combined equivalent z value (z_m) is calculated using x_m and y_m. The tristimulus X and Z values for the final color are

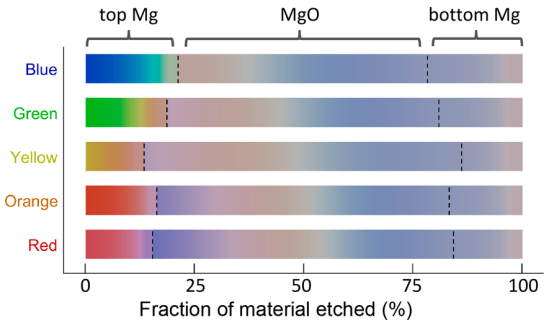

Figure 4. Color tunability with Mg/MgO/Mg MIM structures. Calculations of color change as a function of Mg/MgO/Mg etching in water (the fraction of each specific layer is indicated by dashed lines). Initially, five vivid hues are achieved by varying the ratio between the Mg and MgO layers. Upon exposure to water, the Mg top layer is etched away, resulting in a fast (~8 min) change in hue, which occurs once most of the Mg layer is removed. As the low threshold for Mg is achieved, the original hues are erased and all colors look essentially the same.

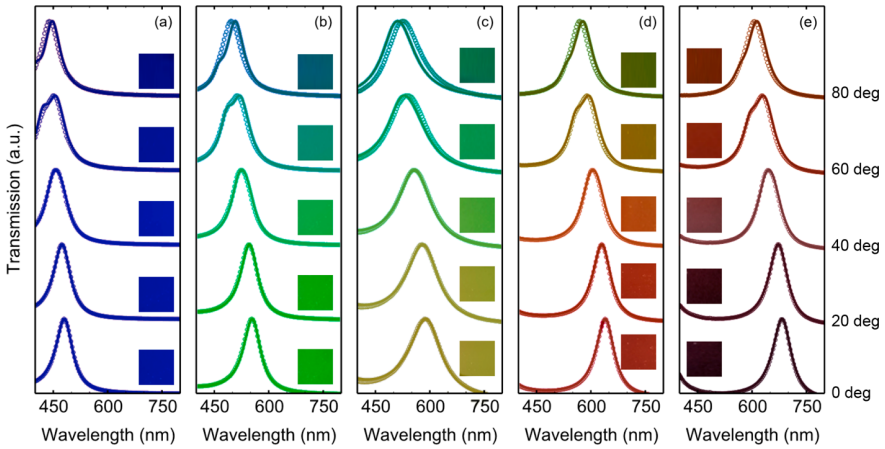

Figure 5. Angular dependence of Mg/MgO/Mg chromaticity. Measured (open circles) and calculated (solid line) transmission spectra of MIM color pixels for MgO thicknesses of (a) 92 nm, (b) 114 nm, (c) 120 nm, (d) 140 nm, and (e) 153 nm as the orientation of the incident light is rotated from 0 (normal incidence) to 80 degrees. The insets are photographs of the fabricated samples.

DOI: 10.1021/acsphotonics.8b01299
ACS Photonics 2019, 6, 272−278

then calculated, where Y affects both X and Z. Therefore, any choice of Y will result in a tristimulus XYZ triplet corresponding to the same color because these quantities are directly proportional. Only the luminance of the final color will be changed with the choice of Y as long as X and Z follow the same proportionality to Y, as described by the following relations:

$$X = \frac{x}{y}Y \text{ and } Z = \frac{z}{y}Y$$

These XYZ tristimulus quantities are then converted to sRGB hues using a 3 × 3 matrix with standard values corresponding to the conversion between the two sets. Note that this method can produce negative R, G, and B coordinates if the determined color lies outside of the sRGB gamut. In this case, they must be replaced with "zero" in order to produce sRGB triplets capable of being ultimately displayed. While the new triplets are not an exact representation of the MIM stack in these situations, they provide an accurate depiction of a similar color (i.e., a blue hue outside of the sRGB gamut still appears as blue inside the sRGB gamut using the new triplet).

All vivid colors for the Mg/MgO/Mg pixels persist even for oblique light incidence. Up to 40 degrees, they have essentially the same sRGB coordinates; the photographs and the transmission data as a function of angle are displayed in Figure 5. For blue, Figure 5(a), the hue is unchanged up to 40 degrees. Beyond that, there is a modest shift in the transmission peak to shorter wavelengths, resulting in a darker hue. The originally green pixel behaves in a similar manner (see Figure 5(b)): for angles above 40 degrees, its color changes to teal, with a concomitant broadening of the transmission peak. The yellow pixel is highly dependent on the angle of incidence. As shown in Figure 5(c), the hues change from yellow (0 to 20 degrees), to light green (40 to 60 degrees), to emerald green (at 80 degrees). The oblique angles also affect the transmission of the originally orange color pixel (see Figure 5(d)), which transitions to very dark yellow and then green at 60 and 80 degrees, respectively. Following the same trend as all other samples, the transmission peak of the dark red pixel also shifts as a function of incident light, as presented in Figure 5(e). Our measurements and calculations are in excellent agreement and display the overall consistent shift in transmission to shorter wavelengths as the angle of incidence increases.

We show that optical transience can be achieved using an earth-abundant, nontoxic, and CMOS-compatible metal with very low optical losses: Mg. To demonstrate this new concept, we fabricate color pixels covering the sRGB color space that "disappear" quickly when exposed to water. While our approach relies on the device's exposure to water, this reconfigurable optical behavior can be controlled by varying the temperature and pH of the water (key parameters). Experiments to determine their relation to the etching rate and, therefore, the precise time-dependent response are planned for the near future. Although the dynamic optical response reported here is irreversible, it exclusively encompasses low-cost materials (Mg and MgO), which significantly facilitates scalability. The nonreversible chemical reactions between water and both Mg and MgO are an advantageous feature in situations where highly sensitive information must be completely erased, ideal for encryption. In environmental science, Mg-based chemical sensors would safely degrade in the landfill after stable operation. Concerning biocompatible systems, contact lenses containing Mg metasurfaces could be implemented for low-cost, portable devices for short-term augmented reality experiences.[46] Moreover, Mg and MgO are also suitable for implanted optical responses (e.g., sensors), where no additional medical procedure would be needed to remove them from a patient's body.

In conclusion, we have demonstrated a novel paradigm for transient photonics based on inorganic materials: Mg and MgO. We showed how vivid color pixels covering the entire sRGB color gamut can be achieved by simply varying the ratio between the thicknesses of the metal and the dielectric layers. Due to the unique chemical reactions of Mg and MgO with water, the color of the pixels disappears completely after 8 min of exposure to water at ambient conditions, enabling (irreversible) reconfigurability. The fabricated hues are robust up to ∼40 degrees of light incidence, shifting to darker colors as the angle of illumination increases, while preserving their intense brightness. This approach can be expanded to the fabrication of dynamic devices based on Mg and MgO nanostructures, such as optical modulators, split ring resonators, and metasurfaces with tunable chirality. Thus, our work represents a critical step toward the field of transient photonics, where there is a pressing need for the realization of portable devices with dynamic optical response for energy, healthcare, and defense applications. We foresee our new and versatile material combination becoming a platform for transient and biocompatible photonic devices for operation in the UV-IR range of the electromagnetic spectrum, possibly expanding to the THz regime.

METHODS

Sample Fabrication. All films were fabricated by RF sputtering deposition (AJA ATC 1800 sputtering unit) and by e-beam evaporation (custom-built Denton Ebeam/thermal evaporator) of Mg and MgO, respectively, at room temperature, with deposition rates of 2.3 and 1.0 Å/s, onto 1 × 1 in.^{2} glass slides. In both cases, we used 99.9% pure sources. The glass slides (substrates) were cleaned with acetone, 2-propanol, and DI water and then dried with N_2, prior to physical deposition. Once removed from the thin-film deposition chambers, the filters were characterized by transmission measurements.

Transmission Measurements/Calculations. These measurements were performed using a variable-angle spectroscopic ellipsometer (M-2000 ellipsometer from J.A. Woollam) containing a light source with a wavelength range of 193−1690 nm. Although Mg easily oxidizes, we observed a negligible change in the permittivity of Mg thin films 4 weeks after fabrication. The baseline for all transmission measurements was in air, and the angular dependence was obtained by rotating the samples from 0 (normal incidence) to 80 degrees in 20-degree increments, while keeping both the light source and the detector fixed. Color matching calculations for mimicking the MIM etching experiments were performed using tristimulus XYZ values from the CIE 1931 standard colorimetric observer data, which provides a coordinate set for wavelengths between 360 and 830 nm in 1 nm increments.

Sample Etching in Water. All color pixels were etched in water simultaneously. The samples were loaded into a holder and submerged in DI water, at room temperature and neutral pH. During the process, a video was recorded while imaging the transmitted color of the samples. Here, a white light source was used for illuminating all samples.

DOI: 10.1021/acsphotonics.8b01299
ACS Photonics 2019, 6, 272−278

■ ASSOCIATED CONTENT

Supporting Information

The Supporting Information is available free of charge on the ACS Publications website at DOI: 10.1021/acsphotonics.8b01299.

Permittivity of Mg, simulations of electric field distribution within a MIM stack, etching of Mg film in water (PDF)

Video of transient chromaticity (AVI)

■ AUTHOR INFORMATION

Corresponding Author

*E-mail: mleite@umd.edu.

ORCID

Chen Gong: 0000-0003-3302-7675

Marina S. Leite: 0000-0003-4888-8195

Notes

The authors declare no competing financial interest.

■ ACKNOWLEDGMENTS

The authors gratefully acknowledge the financial support from NSF (DMR award 1609414), ARO (W911NF1810177), the 2018 Clark Fellowship, and the 2017−2018 Harry K. Wells Graduate Fellowship. The authors also thank Alan Kaplan for instrumentation assistance, Jeremy N. Munday for comments, and the Maryland NanoCenter for its infrastructure and technical support.

■ REFERENCES

(1) Olson, J.; Manjavacas, A.; Liu, L.; Chang, W.-S.; Foerster, B.; King, N. S.; Knight, M. W.; Nordlander, P.; Halas, N. J.; Link, S. Vivid, full-color aluminum plasmonic pixels. *Proc. Natl. Acad. Sci. U. S. A.* **2014**, *111*, 14348−14353.

(2) Heydari, E.; Sperling, J. R.; Neale, S. L.; Clark, A. W. Plasmonic Color Filters as Dual-State Nanopixels for High-Density Microimage Encoding. *Adv. Funct. Mater.* **2017**, *27*, 1701866.

(3) Duempelmann, L.; Casari, D.; Luu-Dinh, A.; Gallinet, B.; Novotny, L. Color Rendering Plasmonic Aluminum Substrates with Angular Symmetry Breaking. *ACS Nano* **2015**, *9*, 12383−12391.

(4) Zhou, W.; Dridi, M.; Suh, J. Y.; Kim, C. H.; Co, D. T.; Wasielewski, M. R.; Schatz, G. C.; Odom, T. W. Lasing action in strongly coupled plasmonic nanocavity arrays. *Nat. Nanotechnol.* **2013**, *8*, 506.

(5) Oulton, R. F.; Sorger, V. J.; Zentgraf, T.; Ma, R.-M.; Gladden, C.; Dai, L.; Bartal, G.; Zhang, X. Plasmon lasers at deep subwavelength scale. *Nature* **2009**, *461*, 629.

(6) Dias, M. R. S.; Gong, C.; Benson, Z. A.; Leite, M. S. Lithography-free, omnidirectional, CMOS-compatible AlCu alloys for thin film superabsorbers. *Adv. Opt. Mater.* **2018**, *6*, 1700830.

(7) Liu, X.; Starr, T.; Starr, A. F.; Padilla, W. J. Infrared spatial and frequency selective metamaterial with near-unity absorbance. *Phys. Rev. Lett.* **2010**, *104*, 207403.

(8) Ra'di, Y.; Simovski, C. R.; Tretyakov, S. A. Thin Perfect Absorbers for Electromagnetic Waves: Theory, Design, and Realizations. *Phys. Rev. Appl.* **2015**, *3*, No. 037001.

(9) Munday, J. N.; Atwater, H. A. Large Integrated Absorption Enhancement in Plasmonic Solar Cells by Combining Metallic Gratings and Antireflection Coatings. *Nano Lett.* **2011**, *11*, 2195−2201.

(10) Pillai, S.; Catchpole, K. R.; Trupke, T.; Green, M. A. Surface plasmon enhanced silicon solar cells. *J. Appl. Phys.* **2007**, *101*, No. 093105.

(11) Dunkelberger, A. D.; Ellis, C. T.; Ratchford, D. C.; Giles, A. J.; Kim, M.; Kim, C. S.; Spann, B. T.; Vurgaftman, I.; Tischler, J. G.; Long, J. P.; Glembocki, O. J.; Owrutsky, J. C.; Caldwell, J. D. Active tuning of surface phonon polariton resonances via carrier photoinjection. *Nat. Photonics* **2018**, *12*, 50−56.

(12) Ou, J. Y.; Plum, E.; Jiang, L.; Zheludev, N. I. Reconfigurable Photonic Metamaterials. *Nano Lett.* **2011**, *11*, 2142−2144.

(13) Suess, R. J.; Bingham, N. S.; Charipar, K. M.; Kim, H.; Mathews, S. A.; Piqué, A.; Charipar, N. A. Ultrafast Phase Transition Dynamics in Strained Vanadium Dioxide Films. *Adv. Mater. Interfaces* **2017**, *4*, 1700810.

(14) Liu, M.; Sternbach, A. J.; Wagner, M.; Slusar, T. V.; Kong, T.; Bud'ko, S. L.; Kittiwatanakul, S.; Qazilbash, M. M.; McLeod, A.; Fei, Z.; Abreu, E.; Zhang, J.; Goldflam, M.; Dai, S.; Ni, G.-X.; Lu, J.; Bechtel, H. A.; Martin, M. C.; Raschke, M. B.; Averitt, R. D.; Wolf, S. A.; Kim, H.-T.; Canfield, P. C.; Basov, D. N. Phase transition in bulk single crystals and thin films of VO2 by nanoscale infrared spectroscopy and imaging. *Phys. Rev. B: Condens. Matter Mater. Phys.* **2015**, *91*, 245155.

(15) Duan, X.; Kamin, S.; Liu, N. Dynamic plasmonic colour display. *Nat. Commun.* **2017**, *8*, 14606.

(16) Palm, K. J.; Murray, J. B.; Narayan, T. C.; Munday, J. N. Dynamic Optical Properties of Metal Hydrides. *ACS Photonics* **2018**, *5* (11), 4677−4686.

(17) Sanz, J.; Ortiz, D.; Alcaraz De La Osa, R.; Saiz, J.; González, F.; Brown, A.; Losurdo, M.; Everitt, H.; Moreno, F. UV plasmonic behavior of various metal nanoparticles in the near-and far-field regimes: geometry and substrate effects. *J. Phys. Chem. C* **2013**, *117*, 19606−19615.

(18) Schulz, L. G. The Optical Constants of Silver, Gold, Copper, and Aluminum. I. The Absorption Coefficient k. *J. Opt. Soc. Am.* **1954**, *44*, 357−362.

(19) Gong, C.; Leite, M. S. Noble Metal Alloys for Plasmonics. *ACS Photonics* **2016**, *3*, 507−513.

(20) Gong, C.; Kaplan, A.; Benson, Z. A.; McClure, J. P.; Baker, D. R.; Rocha, A. R.; Leite, M. S. Band Structure Engineering by Alloying for Photonics. *Adv. Opt. Mater.* **2018**, *6*, 1800218.

(21) Gong, C.; Dias, M. R. S.; Wessler, G. C.; Taillon, J. A.; Salamanca-Riba, L. G.; Leite, M. S. Near-Field Optical Properties of Fully Alloyed Noble Metal Nanoparticles. *Adv. Opt. Mater.* **2017**, *5*, 1600568.

(22) Hashimoto, Y.; Seniutinas, G.; Balčytis, A.; Juodkazis, S.; Nishijima, Y. Au-Ag-Cu nano-alloys: tailoring of permittivity. *Sci. Rep.* **2016**, *6*, 25010.

(23) Blaber, M. G.; Arnold, M. D.; Ford, M. J. A review of the optical properties of alloys and intermetallics for plasmonics. *J. Phys.: Condens. Matter* **2010**, *22*, 143201.

(24) Naik, G. V.; Shalaev, V. M.; Boltasseva, A. Alternative plasmonic materials: beyond gold and silver. *Adv. Mater.* **2013**, *25*, 3264−94.

(25) Castro-Lopez, M.; Brinks, D.; Sapienza, R.; van Hulst, N. F. Aluminum for Nonlinear Plasmonics: Resonance-Driven Polarized Luminescence of Al, Ag, and Au Nanoantennas. *Nano Lett.* **2011**, *11*, 4674−4678.

(26) Knight, M. W.; King, N. S.; Liu, L.; Everitt, H. O.; Nordlander, P.; Halas, N. J. Aluminum for Plasmonics. *ACS Nano* **2014**, *8*, 834−840.

(27) Zhou, L.; Zhang, C.; McClain, M. J.; Manjavacas, A.; Krauter, C. M.; Tian, S.; Berg, F.; Everitt, H. O.; Carter, E. A.; Nordlander, P.; Halas, N. J. Aluminum Nanocrystals as a Plasmonic Photocatalyst for Hydrogen Dissociation. *Nano Lett.* **2016**, *16*, 1478−1484.

(28) Tan, S. J.; Zhang, L.; Zhu, D.; Goh, X. M.; Wang, Y. M.; Kumar, K.; Qiu, C.-W.; Yang, J. K. W. Plasmonic Color Palettes for Photorealistic Printing with Aluminum Nanostructures. *Nano Lett.* **2014**, *14*, 4023−4029.

(29) Akimov, Y. A.; Koh, W. Resonant and nonresonant plasmonic nanoparticle enhancement for thin-film silicon solar cells. *Nanotechnology* **2010**, *21*, 235201.

(30) Johnson, B. M.; Berkel, Z. E. *Biodegradable Materials: Production, Properties, and Applications (Materials Science and Technologies)*; Nova Science Publishers: UK, 2011.

DOI: 10.1021/acsphotonics.8b01299
ACS Photonics 2019, 6, 272−278

(31) Caixeiro, S.; Gaio, M.; Marelli, B.; Omenetto, F. G.; Sapienza, R. Silk-Based Biocompatible Random Lasing. *Adv. Opt. Mater.* **2016**, *4*, 998−1003.
(32) Kwon, H.; Kim, S. Chemically Tunable, Biocompatible, and Cost-Effective Metal−Insulator−Metal Resonators Using Silk Protein and Ultrathin Silver Films. *ACS Photonics* **2015**, *2*, 1675−1680.
(33) Lee, M.; Jeon, H.; Kim, S. A Highly Tunable and Fully Biocompatible Silk Nanoplasmonic Optical Sensor. *Nano Lett.* **2015**, *15*, 3358−3363.
(34) Camposeo, A.; Del Carro, P.; Persano, L.; Cyprych, K.; Szukalski, A.; Sznitko, L.; Mysliwiec, J.; Pisignano, D. Physically Transient Photonics: Random versus Distributed Feedback Lasing Based on Nanoimprinted DNA. *ACS Nano* **2014**, *8*, 10893−10898.
(35) Appusamy, K.; Blair, S.; Nahata, A.; Guruswamy, S. Low-loss magnesium films for plasmonics. *Mater. Sci. Eng., B* **2014**, *181*, 77−85.
(36) Jiao, X.; Wang, Y.; Blair, S. UV fluorescence enhancement by Al and Mg nanoapertures. *J. Phys. D: Appl. Phys.* **2015**, *48*, 184007.
(37) Biggins, J. S.; Yazdi, S.; Ringe, E. Magnesium Nanoparticle Plasmonics. *Nano Lett.* **2018**, *18*, 3752−3758.
(38) Sterl, F.; Strohfeldt, N.; Walter, R.; Griessen, R.; Tittl, A.; Giessen, H. Magnesium as novel material for active plasmonics in the visible wavelength range. *Nano Lett.* **2015**, *15*, 7949−7955.
(39) Palik, E. D. *Handbook of Optical Constants of Solids*; Academic Press, 1998; Vol. 3.
(40) Li, Z.; Butun, S.; Aydin, K. Large-Area, Lithography-Free Super Absorbers and Color Filters at Visible Frequencies Using Ultrathin Metallic Films. *ACS Photonics* **2015**, *2*, 183−188.
(41) Raj Shrestha, V.; Lee, S.-S.; Kim, E.-S.; Choi, D.-Y. Polarization-tuned Dynamic Color Filters Incorporating a Dielectric-loaded Aluminum Nanowire Array. *Sci. Rep.* **2015**, *5*, 12450.
(42) Song, M.; Li, X.; Pu, M.; Guo, Y.; Liu, K.; Yu, H.; Ma, X.; Luo, X. Color display and encryption with a plasmonic polarizing metamirror. *Nanophotonics* **2018**, *7*, 323.
(43) Shaltout, A. M.; Kim, J.; Boltasseva, A.; Shalaev, V. M.; Kildishev, A. V. Ultrathin and multicolour optical cavities with embedded metasurfaces. *Nat. Commun.* **2018**, *9*, 2673.
(44) Zhu, X.; Yan, W.; Levy, U.; Mortensen, N. A.; Kristensen, A. Resonant laser printing of structural colors on high-index dielectric metasurfaces. *Science Advances* **2017**, *3*, No. e1602487.
(45) Viveash, J. P.; Laycock, J. Computation of the resultant chromaticity coordinates and luminance of combined and filtered sources in display design. *Displays* **1983**, *4*, 17−23.
(46) Colburn, S.; Zhan, A.; Majumdar, A. In *Metasurface-based freeform optics for biosensing and augmented reality systems*; 2016 Conference on Lasers and Electro-Optics (CLEO), 5−10 June 2016; 2016; pp 1−2.

DOI: 10.1021/acsphotonics.8b01299
ACS Photonics 2019, 6, 272−278